

1
2 Spontaneous Hot Flow Anomalies at Quasi-Parallel
3 Shocks: 2. Hybrid Simulations
4

5
6 N. Omidi¹, H. Zhang², D. Sibeck³ and D. Turner⁴
7
8
9

- 10 1. Solana Scientific Inc.
11 2. University of Alaska, Fairbanks
12 3. NASA/GSFC
13 4. IGPP/UCLA
14
15
16
17
18
19
20
21
22
23
24
25
26
27
28
29
30
31
32
33

34 Submitted to Journal of Geophysical Research, 2012
35
36
37
38
39
40
41
42
43
44

45
46
47
48
49
50
51
52
53
54
55
56
57
58
59
60
61
62
63
64
65
66
67
68
69

ABSTRACT

Motivated by recent THEMIS observations, this paper uses 2.5-D electromagnetic hybrid simulations to investigate the formation of Spontaneous Hot Flow Anomalies (SHFA) upstream of quasi-parallel bow shocks during steady solar wind conditions and in the absence of discontinuities. The results show the formation of a large number of structures along and upstream of the quasi-parallel bow shock. Their outer edges exhibit density and magnetic field enhancements, while their cores exhibit drops in density, magnetic field, solar wind velocity and enhancements in ion temperature. Using virtual spacecraft in the simulation, we show that the signatures of these structures in the time series data are very similar to those of SHFAs seen in THEMIS data and conclude that they correspond to SHFAs. Examination of the simulation data shows that SHFAs form as the result of foreshock cavitons interacting with the bow shock. Foreshock cavitons in turn form due to the nonlinear evolution of ULF waves generated by the interaction of the solar wind with the backstreaming ions. Because foreshock cavitons are an inherent part of the shock dissipation process, the formation of SHFAs is also an inherent part of the dissipation process leading to a highly non-uniform plasma in the quasi-parallel magnetosheath including large scale density and magnetic field cavities.

INTRODUCTION

70

71

72 Collisionless dissipation processes at the bow shock result in reflection and/or
73 leakage of ions into the upstream region forming the ion foreshock region (Asbridge et
74 al., 1968; Greenstadt et al., 1968;1980; Gosling et al., 1978; Paschmann et al., 1979;
75 Bonifazi et al., 1980a,b). The ion foreshock is populated with a variety of ULF waves
76 (e.g. Russell and Hoppe 1983; Le and Russell, 1992; Greenstadt et al., 1995) with wave
77 vectors towards the sun but carried back by the solar wind in the opposite direction. Both
78 observations and theoretical studies have also established the turbulent nature of the
79 quasi-parallel shocks and the cyclic reformation of the shock front (e.g. Greenstadt et al.,
80 1977, 1993; Russell, 1988, Thomsen et al., 1988, Thomsen et al., 1990a,b; Burgess 1989;
81 Thomas et al., 1990; Winske et al., 1990; Omid et al, 1990; Scholer et al., 1993). This
82 behavior is thought to be caused by the convection of upstream generated ULF waves
83 into the shock.

84

85 In an accompanying paper, Zhang et al. [2012] use THEMIS multi-spacecraft
86 measurements to identify a new structure at the quasi-parallel bow shock named
87 Spontaneous Hot Flow Anomaly (SHFA). SHFAs and Hot Flow Anomalies (HFAs)
88 exhibit similar signatures in spacecraft time series data that consist of enhancements in
89 density and magnetic field in the outer part and depletions in these parameters in the core
90 which is also associated with increased temperature and deflected solar wind flow.
91 However, while HFAs form due to the interaction of solar wind discontinuities with the
92 bow shock (e.g. Schwartz et al., 1988;1995;2000; Thomsen et al., 1986;1988;1993;

93 Paschmann et al., 1988; Thomas et al., 1991; Sibeck et al., 1998;1999;2000; Lin,
94 1997;2002; Lucek et al., 2004; Omidi and Sibeck, 2007; Facsko et al., 2008; Eastwood et
95 al., 2008; Jacobsen et al., 2009), SHFAs form in the absence of discontinuities. In the
96 past, local and global hybrid (kinetic ions, fluid electrons) simulations have been used
97 successfully to examine the formation and impacts of HFAs at the bow shock (e.g.
98 Thomas et al., 1991; Lin, 1997; 2002 and Omidi and Sibeck, 2007). Motivated by SHFA
99 observations, we have conducted an investigation of the quasi-parallel bow shock using
100 global hybrid simulations. As we demonstrate here, simulations show the formation of
101 copious structures at the quasi-parallel bow shock and foreshock whose time series
102 signatures resemble those of SHFAs presented by Zhang et al. [2012]. The results
103 indicate that SHFAs are an inherent part of the super-critical quasi-parallel shock
104 dissipation processes and result in highly turbulent and non-uniform magnetosheath
105 plasma.

106

107 The structure of the paper is as follows. Section 2 describes the hybrid model used in
108 this study while the simulation results are described in section 3. Section 4 provides a
109 summary and conclusions.

110

111 2. HYBRID SIMULATION MODEL

112

113

114 The main tool of investigation in this study is a 2.5-D (2-D in space and 3-D in
115 currents and electromagnetic fields) global hybrid simulation model used extensively in
116 the past (e.g. Omidi et al., 2004, 2005, 2006, 2009a,b; 2010; Omidi and Sibeck, 2007;
117 Blanco-Cano et al., 2006a,b, 2009, 2011; Sibeck et al., 2008). In electromagnetic hybrid

118 codes, ions are treated as macro-particles and consist of one or more species (e.g.,
119 differing mass, charge, etc.) whereas electrons are treated as a massless, charge
120 neutralizing fluid (see e.g. Winske and Omid, 1993, 1996).

121

122 The model consists of a dipole inside a sphere whose surface represents the
123 ionospheric boundary. A solar wind type plasma with electron and ion betas (ratio of
124 thermal to magnetic pressure) of 0.3 each and flow speed of $12 V_A$ (Alfven speed) is
125 uniformly loaded in the system except for the region inside the ionospheric boundary.
126 This plasma is continuously injected from the left hand boundary throughout the whole
127 run. The remaining boundaries remain open for the plasma to leave. Similarly, open
128 boundary conditions are applied for the electromagnetic fields so that excited waves and
129 turbulence in the system leave through these boundaries. The simulation box lies in the
130 X-Z (noon-midnight meridian) plane with X along the solar wind flow direction (Sun-
131 Earth line) and the magnetic dipole moment in the Z direction so that X corresponds to $-$
132 X_{GSM} and Z corresponds to Z_{GSM} . The simulation box extends 1500 ion skin depths c/ω_p
133 (where c is the speed of light and ω_p is the ion plasma frequency) in the X and Z
134 directions with cell size of 1 ion skin depth. The interplanetary magnetic field (IMF) lies
135 in the X-Z plane and makes a cone angle of 10° with the X axis. To optimize the
136 computational resources, the simulated magnetosphere is smaller (by a factor of ~ 5) than
137 the Earth's magnetosphere. On the other hand, the simulated plasma parameters and
138 characteristic time and spatial scales such as gyroperiod, or ion skin depth are the same as
139 in the solar wind and magnetosphere. This ensures that the simulations are capable of
140 generating plasma and field values and characteristic scales that can be directly compared

141 to observations at the Earth's bow shock. As demonstrated in our earlier studies, the
142 physical processes occurring in smaller bow shocks and magnetospheres are similar to
143 those at the Earth's magnetosphere and much can be learned from these simulations
144 including scaling properties of various magnetospheric processes (e.g. Omidi et al., 2004,
145 2005, 2006, 2009a,b, 2010; Omidi and Sibeck, 2007; Blanco-Cano et al., 2006a,b, 2009,
146 2011; Sibeck et al., 2008).

147

148 3. FORMATION OF SHFAs

149

150 Panel (a) in Figure 1 shows the plasma density (normalized to solar wind value)
151 and magnetic field lines in a portion of the simulation domain. The quasi-perpendicular
152 and parallel portions of the bow shock are labeled in this panel with the latter falling
153 primarily in the southern hemisphere. Also labeled is the ion foreshock, upstream of the
154 quasi-parallel shock, and the Foreshock Compressional Boundary (FCB) that separates a
155 highly disturbed and turbulent ion foreshock plasma from a nearly pristine like solar wind
156 that falls inside the ion foreshock (beam) boundary (see Sibeck et al., 2008; Omidi et al.,
157 2009b). Panel (b) in Figure 1 shows the density zoomed around the quasi-parallel shock
158 and the ion foreshock. The latter includes regions of low density labeled foreshock
159 cavitons. The presence of these structures was predicted by global hybrid simulations
160 (Lin, 2003; Lin and Wang, 2005; Omidi, 2007) and confirmed in the ion foreshock
161 (Blanco-Cano et al., 2009, 2011; Kajdič et al. 2010, 2011). Foreshock cavitons are about
162 an R_E (Earth radii) in size and are associated with drops in density and magnetic field in
163 their core by as much as 50% or more and plasma and magnetic field enhancements in

164 their outer edge. They form as a result of the nonlinear evolution of ULF waves and are
165 carried back by the solar wind towards the bow shock. As we show here, the interaction
166 between foreshock cavitons and the bow shock is highly significant and an inherent part
167 of the quasi-parallel shock dissipation processes.

168

169 Although at any given time the structure of the quasi-parallel bow shock is highly
170 turbulent, a closer examination reveals processes that occur at and upstream of the shock
171 on a regular basis. An example of this is illustrated in Figures 2 and 3 that show the
172 density and ion temperature (normalized to solar wind value) respectively at 4 different
173 times (normalized to proton gyroperiod Ω^{-1}) zoomed around the quasi-parallel bow
174 shock. Ion temperature is obtained by calculating the second moment of the velocity
175 distribution function and includes the effects of the energetic ions in the foreshock. Panel
176 (a) in Figure 2 shows a structure at and upstream of the bow shock consisting of density
177 enhancements surrounding a low density region. Examination of panel (a) in Figure 3
178 shows the ion temperature in the low density region is over 600 times hotter than the
179 pristine solar wind. Note that the ion temperature scale in Figure 3 is set to a maximum
180 of 600 for better clarity. This structure looks similar to a simulated HFAs formed at the
181 bow shock due to solar wind discontinuities, e.g. Omidi and Sibeck [2007]. Panels (b)
182 through (d) in Figures 2 and 3 show the time evolution of this structure that penetrates
183 further into the magnetosheath and eventually becomes a part of the highly non-uniform
184 and turbulent magnetosheath. In the process the energetic ions within the structure are
185 injected into the magnetosheath.

186

187 To see the signature of this structure and its time evolution as might be observed
188 in spacecraft data, Figure 4 shows the ion density, total pressure (normalized to solar
189 wind value), velocity (normalized to V_A) and temperature, as well as the magnetic field
190 (normalized to solar wind value) as observed in time at the location marked by “X” in
191 panel (a) of Figure 2. As can be seen, the signature consists of enhancements in density
192 and magnetic field (beginning at time $\sim 250 \Omega^{-1}$) that reach a factor of ~ 3 above the solar
193 wind levels. This is followed by large drops in density (minimum value of $\sim 15\%$ of solar
194 wind density) and field (minimum value of $\sim 30\%$ of solar wind magnetic field) in
195 association with flow deceleration and deflection and enhancements in ion temperature.
196 Note that despite the temperature enhancements, the total pressure in the low density core
197 region is below that in the solar wind. Subsequently, the density and magnetic field
198 increase above the solar wind levels by a factor of ~ 5 before returning to solar wind
199 values. This signature is identical to that of HFAs in general and the SHFAs reported by
200 Zhang et al. [2012]. Given the absence of a solar wind discontinuity in the simulation, we
201 identify this structure as a SHFA.

202

203 To illustrate the formation of this SHFA, Figure 5 shows the total magnetic field,
204 ion temperature and ion velocity in the X direction at two separate times. The top panels
205 show a well developed foreshock caviton upstream of the bow shock. The bottom panels
206 show that the convection of this caviton by the solar wind into the bow shock transforms
207 it into a SHFA. This transformation is associated with further energization of the ions in
208 the core of the caviton and the enhancement of the cavity (reduction in magnetic field and
209 density) which in turn increases the magnetic field and density in the outer parts. The

210 details of the ion velocity distribution functions within the SHFA and their time evolution
211 and their relationship to particle energization process remain to be understood and are
212 under investigation. Preliminary results suggest that ion trapping by the cavitons and also
213 ion reflection between the bow shock and the cavitons may play an important role in the
214 acceleration process. Given the convection of the cavitons towards the bow shock, the
215 back and forth motion of ions between the cavitons and the bow shock can result in
216 particle acceleration through first and second order Fermi processes.

217

218 Examination of the simulation results show that SHFAs form regularly along the
219 quasi-parallel bow shock surface as isolated foreshock cavitons, such as that in Figure 5,
220 encounter the shock. We also find that at times, multiple cavitons arrive at the bow shock
221 near simultaneously and result in the formation of larger and more complex structures.
222 An example of this is illustrated in Figure 6 that shows the density zoomed around the
223 quasi-parallel shock at 4 different times. Panel (a) in Figure 6 shows the presence of a
224 number of SHFA like structures along the bow shock that formed at about the same time
225 due to the arrival of multiple foreshock cavitons at the shock. Panels (b) through (d) show
226 the time evolution of these SHFAs as they penetrate into the magnetosheath and result in
227 large inhomogeneities and turbulence in the quasi-parallel magnetosheath.

228

229 Figure 7 shows the signature of this event in time series data as observed at points “A”,
230 “B”, “C” and “D” shown in panel (a) of Figure 6. Density, magnetic field and
231 temperature are normalized to solar wind values and flow speed is normalized to the
232 Alfvén speed in the solar wind. The data looks quite different at each observing point. At

233 point “A”, the data shows signatures associated with 2 SHFAs that are shaded. At point
234 “B” two shaded signatures are present that show density and field enhancements and
235 depletions, flow deceleration and the presence of energetic ions and look similar to
236 SHFAs, however, some differences to SHFAs can also be observed. Similarly, at points
237 “C” and “D” signatures similar to SHFAs are present (shaded regions) but clean and full
238 signatures of SHFAs are harder to identify. In effect the presence of multiple SHFAs at
239 the bow shock and their mutual interactions result in highly nonlinear and complex
240 structures whose signatures in spacecraft data would be similarly complex and hard to
241 decipher.

242

243
244

5. SUMMARY AND CONCLUSIONS

245 Motivated by the multi-spacecraft THEMIS observations of Spontaneous Hot
246 Flow Anomalies at the quasi-parallel bow shock, by Zhang et al. [2012] we have
247 examined the structure of a super-critical quasi-parallel bow shock using global hybrid
248 simulations. The results show the formation of copious structures at the quasi-parallel
249 shock whose time series data resemble those of HFAs and SHFAs. Given the steady
250 nature of the solar wind and the absence of a discontinuity in the simulation, these
251 structures are identified as SHFAs. The formation of SHFAs in the simulation is tied to
252 the convection of foreshock cavitons by the solar wind and their interaction with the bow
253 shock. Foreshock cavitons are structures of the order of $\sim 1 R_E$ (Blanco-Cano et al., 2009,
254 2011; Kajdič et al., 2010, 2011) consisting of low density and magnetic field core region
255 populated with energetic ions and an outer layer with increased density and magnetic
256 field strength. Transformation of a caviton to a SHFA is associated with further

257 energization of ions, reductions in density and magnetic field in the core of the cavitons
258 and the enhancements of the density and magnetic field in the outer region. The size of
259 SHFAs in the Z direction is ~ 50 ion skin depths which is comparable to that of foreshock
260 cavitons and is of the order of $1 R_E$ which is also comparable to the size of HFAs at the
261 bow shock.

262

263 Foreshock cavitons have been observed under a wide range of solar wind
264 velocities (Mach number) and IMF orientations. During small and intermediate IMF cone
265 angles when the foreshock falls upstream of the dayside magnetosphere, foreshock
266 cavitons are carried by the solar wind into the bow shock. As a result, we expect the
267 formation of SHFAs at the quasi-parallel bow shock over a wide range of solar wind
268 conditions. Although the simulation results shown here correspond to Alfvén Mach
269 number of 12 and IMF cone angle of 10° , examination of other runs with lower Mach
270 numbers (down to $6 V_A$) and cone angles (smaller than 45°) also shows the formation of
271 SHFAs at the shock. As such, we believe the formation of SHFAs at the quasi-parallel
272 bow shock is a common process and quite significant for ion acceleration and dissipation
273 at the super-critical quasi-parallel bow shock. Similarly, the formation and dissipation of
274 SHFAs as they interact with the bow shock, is critical for determining the properties of
275 the magnetosheath plasma.

276

277 The simulation results also demonstrate that when a number of foreshock cavitons
278 arrive and interact with the bow shock near simultaneously, structures larger and more
279 complex than SHFAs are formed. These structures are influenced by the interaction of the

280 cavitons with the bow shock but also with each other. As a result, the time series data
281 obtained at various points along the bow shock are more complex and varied from point
282 to point and exhibit full or partial signatures of multiple SHFAs. Such interactions also
283 lead to large inhomogeneities in the magnetosheath. The results presented by Zhang et al.
284 [2012] and here demonstrate that ion dissipation processes at the quasi-parallel shock are
285 even more complex than previously thought. Future data analysis and simulations are
286 needed to shine more light on the impacts of SHFAs on the bow shock, magnetosheath
287 and the magnetosphere. Similarly, differences between HFAs and SHFAs and their
288 magnetospheric impacts need to be explored further. The fact that the formation of HFAs
289 is associated with the presence of solar wind discontinuities while SHFAs form due to the
290 interaction of cavitons with the bow shock provide a means of distinguishing between
291 HFAs and SHFAs. For example, Zhang et al. [2012] use the absence of a solar wind
292 discontinuity associated with an event to identify it as an SHFA. As we learn more about
293 SHFAs and how they compare and contrast to HFAs other means of distinguishing
294 between the two may become available.

295

296

297

298

AKNOWLEDGMENTS

299 Work for this project was supported by NSF grants AGS-1007449, AGS-0963111 and

300 AGS-0962815.

301

302

303

304

305

REFERENCES

306 Asbridge, J. R., S. J. Bame, and I. B. Strong (1968), Outward flow of protons from the
307 earth's bow shock, *J. Geophys. Res.*, *73*, 5777.

308

309 Blanco-Cano, X., N. Omidı and C. T. Russell (2006a), Macro-Structure of Collisionless
310 Bow Shocks: 2. **ULF waves in the foreshock and magnetosheath**, *J. Geophys. Res.*, *111*,
311 **A10205**, doi 10.1029/2005JA01142.

312

313 Blanco-Cano, X, N. Omidı, and C. T. Russell (2006b), ULF waves and their influence on
314 bow shock and magnetosheath structures, *Adv Space. Res.*, *37*, 1522, doi:
315 10.1016/j.asr.2005.10.043.

316

317 Blanco-Cano, X., N. Omidı and C. T. Russell (2009), Global hybrid simulations:
318 Foreshock waves and cavitons under radial **interplanetary magnetic field** geometry, *J.*
319 *Geophys. Res.*, *114*, A01216, doi:10.1029/2008JA013406.

320

321 Blanco-Cano, X., P. Kajdič, N. Omidı, and C. T. Russell (2011), Foreshock cavitons for
322 different interplanetary magnetic field geometries: Simulations and observations, **J.**
323 **Geophys. Res.**, *116*, A09101, doi:10.1029/2010JA016413.

324

325 Bonifazi, C., A. Egidi, G. Moreno, and S. Orsini (1980a), Backstreaming ions outside the
326 earth's bow shock and their interaction with the solar wind, *J. Geophys. Res.*, *85*, 3461.

327

328 Bonifazi, C., G. Moreno, A. J. Lazarus, and J. D. Sullivan (1980b), Deceleration of the
329 solar wind in the earth's foreshock region: ISEE 2 and IMP 8 observations, *J. Geophys.*
330 *Res.*, 85, 6031.

331

332 Burgess, D. (1989), On the effect of a tangential discontinuity on ions specularly
333 reflected at an oblique shock, *J. Geophys. Res.*, 94, 472.

334

335 Eastwood, J. P., et al. (2008), Themis observations of a hot flow anomaly: Solar wind,
336 magnetosheath, and ground-based measurements, *Geophys. Res. Lett.*, 35, 332
337 doi:10.1029/2008GL033475.

338

339 Facsko, G., et al. (2008), A statistical study of hot flow anomalies using Cluster data, *Adv*
340 *Space. Res.*, 41 (8), 1286, doi:10.1016/j.asr.2008.02.005.

341

342 Gosling J. T., J. R. Asbridge, S. J. Bame, G. Paschmann, and N. Sckopke (1978),
343 Observations of two distinct populations of bow shock ions in the upstream solar wind, *J.*
344 *Geophys. Res.*, 5, 957.

345

346 Greenstadt, E. W., et al. (1968), Correlated magnetic field and plasma observations of the
347 Earth's bow shock, *J. Geophys. Res.*, 73, 51.

348

349 Greenstadt, E. W., C. T. Russell, V. Formisano et al. (1977), Structure of a quasi-parallel,
350 quasi-laminar bow shock, *J. Geophys. Res.*, 82, 651.

351

352 Greenstadt, E. W., C. T. Russell, and M. Hoppe (1980), Magnetic field orientation and
353 suprathermal ion streams in the earth's foreshock, *J. Geophys. Res.*, 85, 3473.

354

355 Greenstadt, E. W., et al. (1993), The quasiperpendicular environment of large magnetic
356 pulses in Earth's quasi-parallel foreshock: ISEE 1 & 2 observations, *Geophys. Res. Lett.*,
357 20, 1459.

358

359 Greenstadt, E. W., et al. (1995), ULF waves in the foreshock, in *Physics of Collisionless*
360 *Shocks*, ed. C. T. Russell, *Adv Space. Res.*, Pergamon, 71.

361

362 Jacobsen, K. S., et al. (2009), THEMIS observations of extreme magnetopause motion
363 caused by a hot flow anomaly, *J. Geophys. Res.*, 114, doi:10.1029/2008JA013873.

364

365 Kajdič, P., X. Blanco-Cano, N. Omid, and C. T. Russell (2010), Analysis of waves
366 surrounding the foreshock cavitons, *AIP Conf. Proc.*, 1216, 479, doi:10.1063/1.3395907.

367

368 Kajdič, P., X. Blanco-Cano, N. Omid, and C. T. Russell (2011), Multi-spacecraft study
369 of foreshock cavitons upstream of the quasi-parallel Earth's bow shock, *Planet. Space*
370 *Sci.*, 59, 705, doi:10.1016/j.pss.2011.02.005.

371

372 Le, G. and C. T. Russell (1992), A study of ULF wave foreshock morphology, II: Spatial
373 variations of ULF waves, *Planet. Space Sci.*, 40.

374

375 Lin, Y. (1997), Generation of anomalous flows near the bow shock by its interaction with
376 interplanetary discontinuities, *J. Geophys. Res.*, 102, 24265.

377

378 Lin, Y. (2002), Global hybrid simulation of hot flow anomalies near the bow shock and
379 in the magnetosheath, *Planet. Space Sci.*, 50, 577, 2002.

380

381 Lin Y. (2003), Global-scale simulation of foreshock structures at the quasi-parallel bow
382 shock, *J. Geophys. Res.*, 108, 1390, DOI 10.1029/2003JA009991.

383

384 Lin, Y., and X. Wang (2005), Three-dimensional global hybrid simulation of dayside
385 dynamics associated with the quasiparallel bow shock, *J. Geophys. Res.*, 110, A12216,
386 doi:10.1029/2005JA011243.

387

388 Lucek, E. A., et al. (2004), Cluster observations of hot flow anomalies, *J. Geophys. Res.*,
389 109, A06207, doi:10.1029/2003JA010016.

390

391 Omidi, N. (2007), Formation of cavities in the foreshock, in *Turbulence and Nonlinear*
392 *Processes in Astrophysical Plasmas*, Editors D. Shaikh and G. Zank, AIP Conference
393 Proceedings, 932, 181.

394

395 Omidi, N., and D. G. Sibeck (2007), Formation of hot flow anomalies and solitary
396 shocks, *J. Geophys. Res.*, 112, A01203, doi:10.1029/2006JA011663.

397

398 Omidi, N., K. B. Quest, and D. Winske (1990), Low mach number parallel and quasi-
399 parallel shocks, *J. Geophys. Res.*, **95**, 20,717--20,730.

400

401 Omidi, N., X. Blanco-Cano, C. T. Russell and H. Karimabadi (2004), Dipolar
402 magnetospheres and their characterization as a function of magnetic moment, *Adv. Space*
403 *Res.*, 33, Issue 11, 1996.

404

405 Omidi, N., X. Blanco-Cano and C. T. Russell (2005), Macro-structure of collisionless
406 bow shocks: 1. Scale lengths, *J. Geophys. Res.*, 110, A12212,
407 doi:10.1029/2005JA011169.

408

409 Omidi, N., X. Blanco-Cano, C. T. Russell and H. Karimabadi (2006), Global hybrid
410 simulations of solar wind interaction with Mercury: Magnetospheric boundaries, *Adv.*
411 *Space Res.*, doi:10.1016/j.asr.2005.11.019.

412

413 Omidi, N., T. Phan, and D. G. Sibeck (2009a), Hybrid simulations of magnetic reconnection
414 initiated in the magnetosheath, *J. Geophys. Res.*, 114, A02222, doi:1029/2008JA013647.

415

416 Omidi, N., D. Sibeck and X. Blanco-Cano (2009b), Foreshock compressional boundary,
417 *J. Geophys. Res.*, 114, A08205, doi:10.1029/2008JA013950.

418

419 Omidi, N., J. P. Eastwood, and D. G. Sibeck (2010), Foreshock bubbles and their global
420 magnetospheric impacts, *J. Geophys. Res.*, **115**, A06204.

421

422 Paschmann, G., et al. (1979), Association of low frequency waves with suprathermal ions
423 in the upstream solar wind, *Geophys.Res.Lett.*, 6, 209.

424

425 Paschmann, G., et al. (1988), 3-Dimensional plasma structures with anomalous flow
426 directions near the Earth's bow shock, *J. Geophys. Res.*, 93,11279.

427

428 Russell, C. T. and M. Hoppe (1983), Upstream waves and particles, *Space Sci Revs*, 34,
429 155.

430

431 Russell, C. T. (1988), Multipoint measurements of upstream waves, *Adv. Space Res.*, 8,
432 147.

433

434 Scholer, M., M. Fujimoto and H. Kucharek (1993), 2-dimensional simulations of
435 supercritical quasi-parallel shocks- upstream waves, downstream waves and shock re-
436 formation, *J. Geophys. Res.*, 98, 18971.

437

438 Schwartz, S. J., et al. (1988), Active current sheets near the earth's bow shock, *J.*
439 *Geophys. Res.*, 93,11295.

440

441 Schwartz, S. J. (1995), Hot flow anomalies near the earth's bow shock, in *Physics of*
442 *Collisionless Shocks*, C.T. Russell Editor, Advances in Space Research, Pergamon, 107.

443

444 Schwartz, S. J., et al. (2000), Conditions for the formation of hot flow anomalies, *J.*
445 *Geophys. Res.*, 105, 12639.

446

447 Sibeck, D. G., et al. (1998), Gross deformation of the dayside magnetopause, *Geophys.*
448 *Res.Lett.* , 25 (4), 453.

449

450 Sibeck, D. G., et al. (1999), Comprehensive study of the magnetospheric response to a
451 hot flow anomaly, *J. Geophy. Res.*, 104, 4577.

452

453 Sibeck, D. G., et al. (2000), Magnetopause motion driven by interplanetary magnetic
454 field variations, *J. Geophys. Res.*, 105, 25,155.

455

456 Sibeck, D. G., N. Omidi, I. Dandouras, and E. Lucek (2008), On the edge of the
457 foreshock: model-data comparisons, *Ann. Geophys.*, 26, 1539.

458

459 Thomas, V. A., D. Winske and N. Omidi (1990), Reforming super-critical quasi-parallel
460 shocks, 1. One- and two-dimensional simulations, *J. Geophys. Res.*, 95, 18809.

461

462 Thomas, V. A., D. Winske, M. F. Thomsen and T. G. Onsager (1991), Hybrid simulation
463 of the formation of a hot flow anomaly, *J. Geophys. Res.*, 96, 11625.

464

465 Thomsen, M. F., et al. (1986), Hot diamagnetic cavities upstream from the earth's bow
466 shock, *J. Geophys. Res.*, 91, 2961.

467

468 Thomsen, M. F., et al. (1988), On the origin of hot diamagnetic cavities near the earth's
469 bow shock, *J. Geophys. Res.*, 93, 11311.

470

471 Thomsen, et al. (1990a), Two-state ion heating at quasi-parallel shock, *J. Geophys. Res.*,
472 95, 957.

473

474 Thomsen, M. F., J. T. Gosling, S.J. Bame and C.T. Russell (1990b), Magnetic pulsations
475 at the quasi-parallel shock, *J. Geophys. Res.*, 95, 957.

476

477 Thomsen, M. F., et al. (1993), Observational test of hot flow anomaly formation by the
478 interaction of a magnetic discontinuity with the bow shock, *J. Geophys. Res.*, 98, 15319.

479

480 Winske, D., N. Omid, K. B. Quest, and V. A. Thomas (1990), Reforming
481 supercritical quasi-parallel shocks: 2. Mechanism for wave generation and front
482 reformation, *J. Geophys. Res.*, 95, 18,821.

483

484 Winske, D. and N. Omid (1993), Hybrid codes: Methods and applications, in *Computer*
485 *Space Plasma Physics: Simulation Techniques and Software*, ed. H. Matsumoto & Y.
486 Omura, Terra Scientific, 103.

487

488 Winske, D., and N. Omid (1996), A nonspecialist's guide to kinetic simulations of space
489 plasmas, *J. Geophys. Res.*, 101, 17287.

490

491 Zhang. H., et al. (2012), Spontaneous hot flow anomalies at quasi-parallel shocks: 1.

492 Observations, *J. Geophys. Res.*, submitted.

493

494

495

496

497

498

499

FIGURE CAPTIONS

500 Figure 1. Panel (a) shows the plasma density normalized to solar wind value and marks
501 various parts of the bow shock and the ion foreshock. Panel (b) zooms closer into the
502 foreshock and bow shock showing foreshock cavitons.

503

504 Figure 2. Plasma density normalized to solar wind value at 4 times (proton gyroperiods
505 Ω^{-1}) demonstrating the interaction of SHFA with the bow shock.

506

507 Figure 3. Ion temperature normalized to solar wind value at 4 times demonstrating
508 injection of energetic ions into the magnetosheath by SHFA.

509

510 Figure 4. Time series data showing plasma density, three components of velocity and
511 magnetic field and ion temperature generated at the point marked by “X” in panel (a) of
512 Figure 2. Density, total pressure, magnetic field and temperature are normalized to solar
513 wind values and velocities are normalized to the Alfvén speed in the solar wind. The data
514 shows signatures of a SHFA.

515

516 Figure 5. Total magnetic field, ion temperature and velocity in X direction are shown at
517 two times demonstrating the transformation of a foreshock caviton into a SHFA.

518

519 Figure 6. Plasma density at 4 times showing the evolution of a number of SHFAs as they
520 interact with the bow shock and eventually end up in the magnetosheath.

521

522 Figure 7. Time series data showing the variations of total magnetic field, flow speed
523 along X, ion temperature and density at points A, B, C and D marked in panel (a) of
524 Figure 6. Density, magnetic field and temperature are normalized to solar wind values
525 and flow speed is normalized to the Alfvén speed in the solar wind.

526

527

528

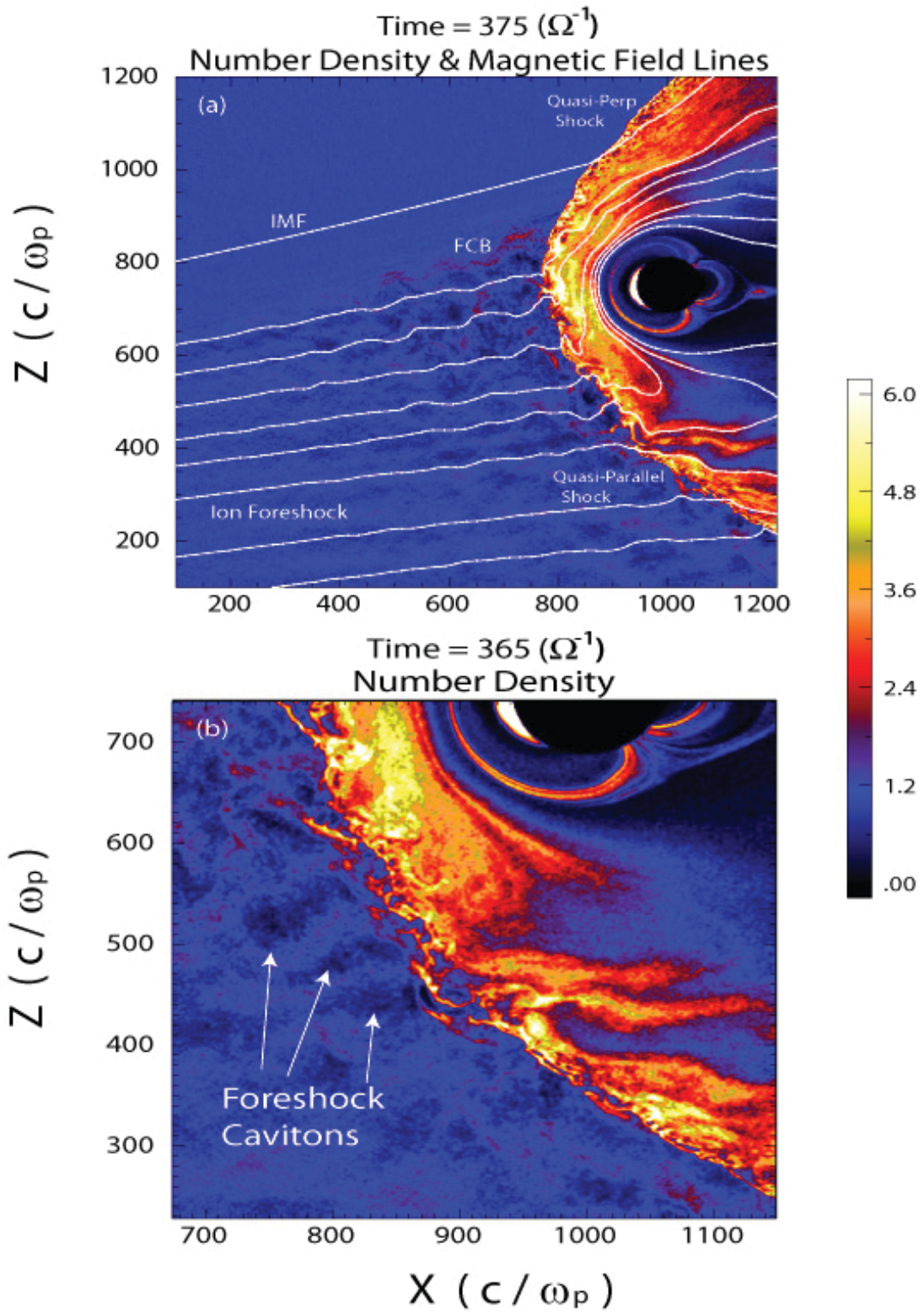
529

530

531

532

533
534
535
536
537
538
539
540
541
542
543
544
545
546
547
548
549
550
551
552
553
554
555
556
557
558
559
560
561
562
563
564
565
566
567
568
569
570
571



572
573
574

Fig. 1

575
576
577
578
579
580

Number Density

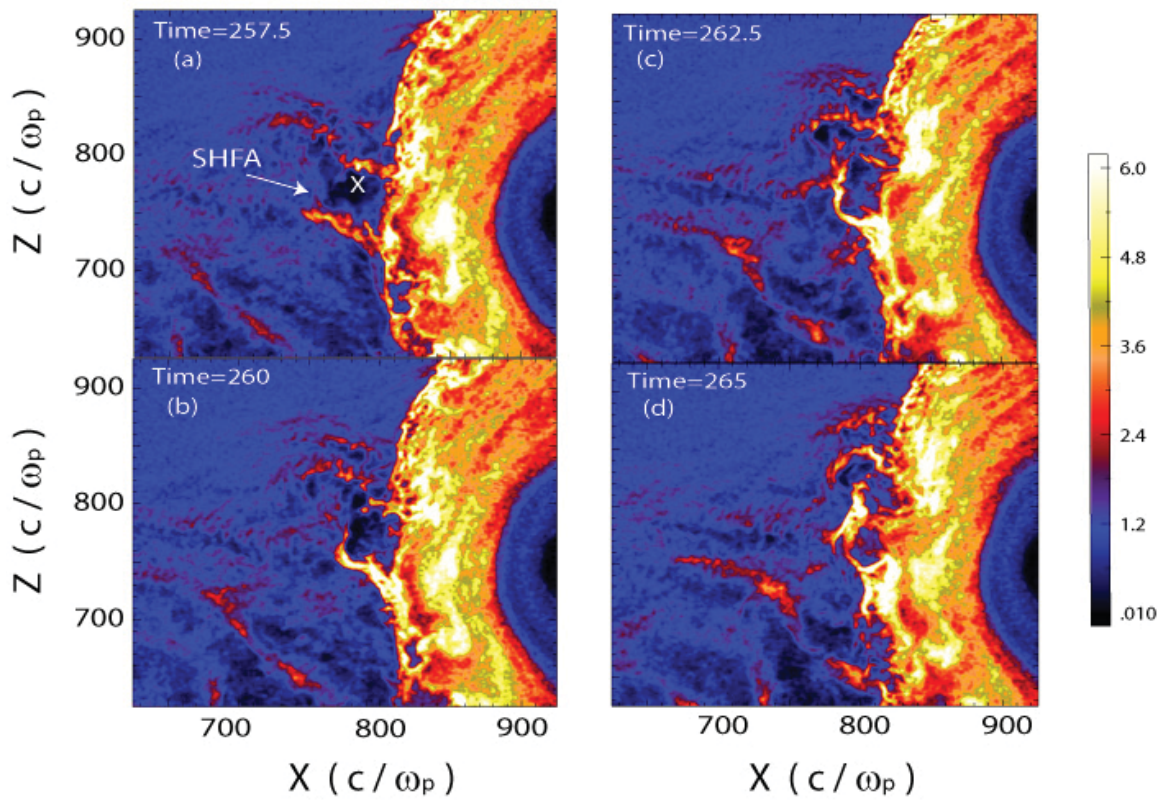
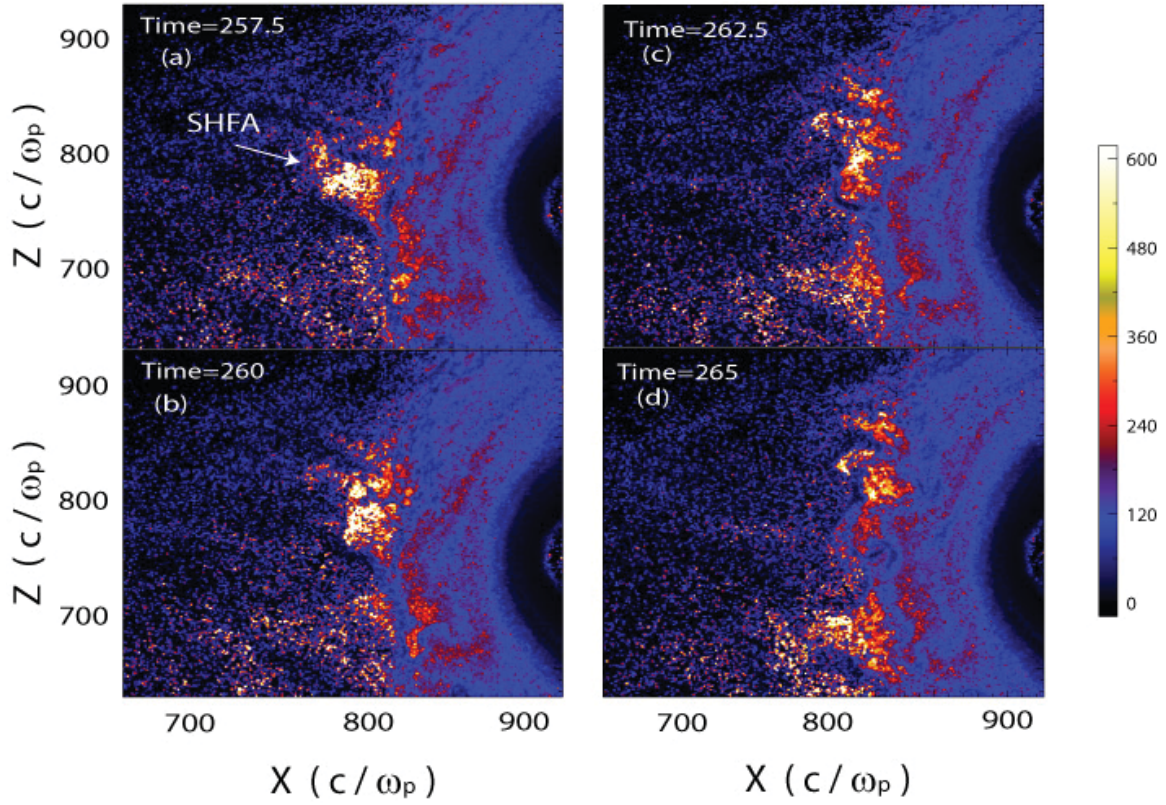


Fig. 2

581
582
583
584
585
586
587
588
589
590
591
592
593
594
595
596
597

598
599
600
601
602
603

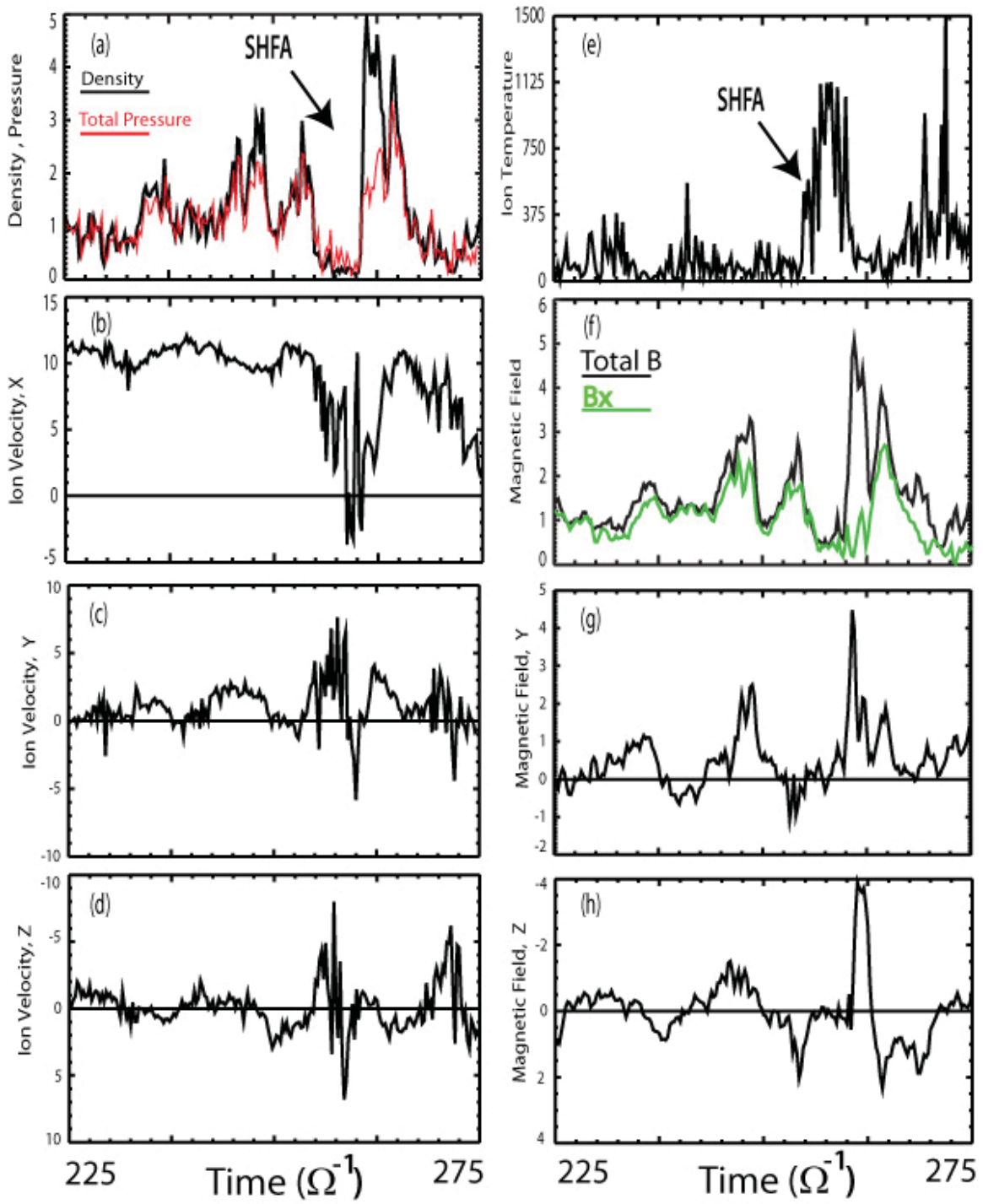
Temperature



604
605
606
607
608
609
610
611
612
613
614
615
616
617
618
619
620

Fig. 3

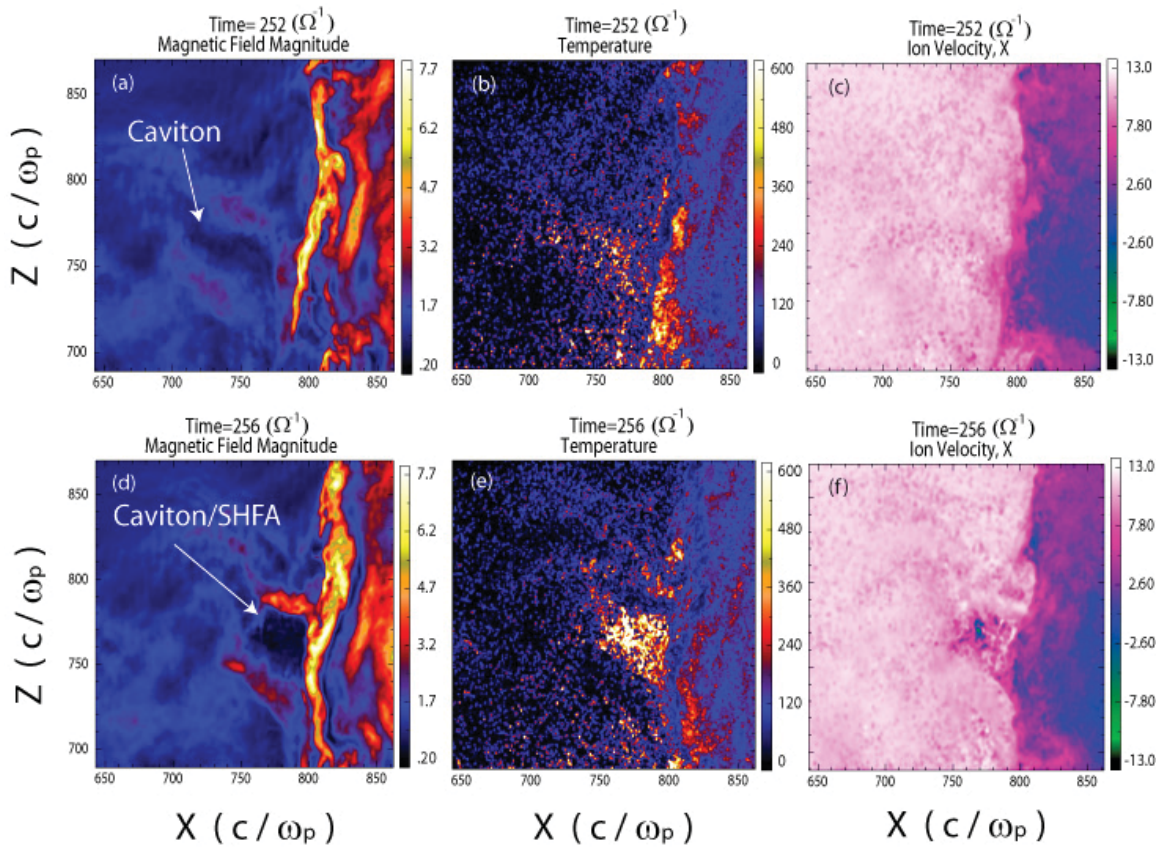
621
622
623
624



625
626
627
628
629

Fig. 4

630
631
632
633
634
635
636
637
638
639
640
641

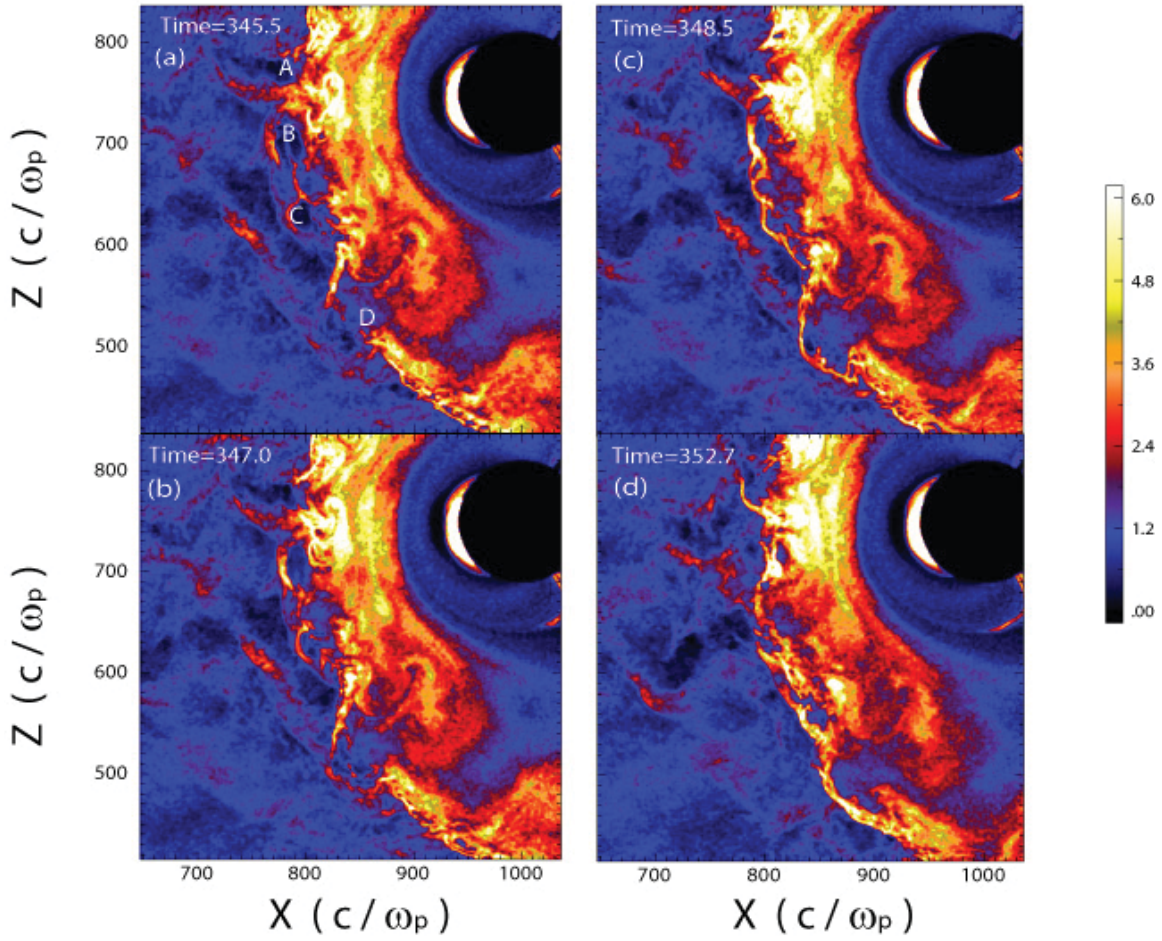


642
643
644
645
646
647
648
649
650
651
652
653

Fig. 5

654
655
656
657

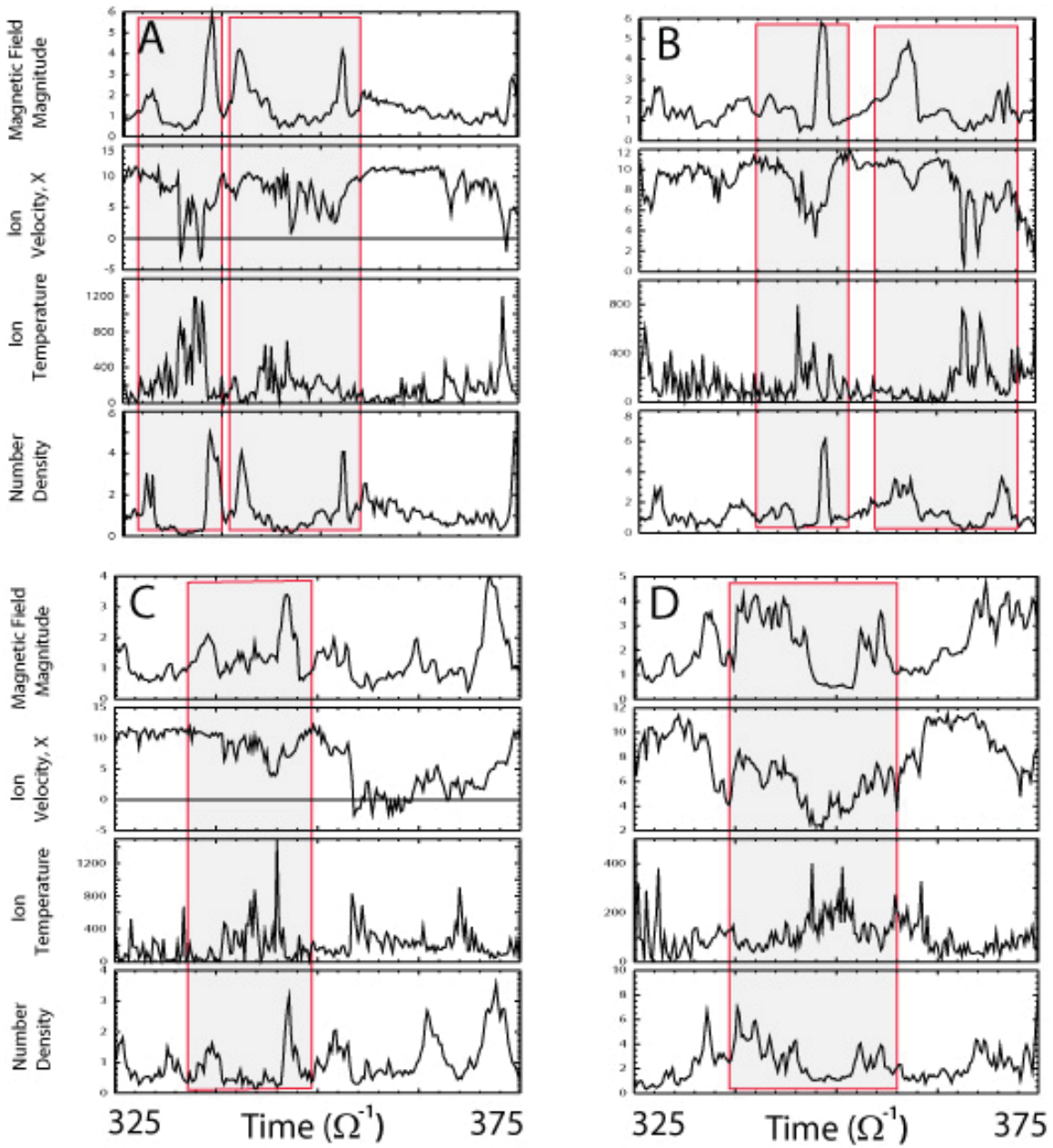
Number Density



658
659
660
661
662
663
664
665
666
667
668
669
670
671
672
673

Fig. 6

674
675
676
677



678
679
680
681
682
683
684

Fig. 7